ORIGINAL ARTICLE

The drying characteristics of wheat straw in a self-designed pilot-scale cyclone dryer

Zhixiong Zhou[1] · Yinhai Su[1] · Sheng Wang[2] · Qi Cao[1] · Huiyan Zhang[1]

Abstract

Biomass is normally a poor thermal conductor with high moisture content. These characteristics not only reduce the calorific value of biomass, but also promote the formation of coke and non-condensable gas during subsequent thermal processing. However, the commercial application of biomass is limited to the high energy and time consumption during drying stage. In this research, a pilot-scale cyclone dryer was designed for efficient drying of biomass and the drying characteristics were explored. Its superiority was revealed via the comparison of two traditional drying methods as blast drying oven and fluidized bed. Results showed that cyclone drying has the highest moisture diffusion coefficient (9.0×10^{-10} m^2/s to 1.3×10^{-9} m^2/s) and the lowest drying activation energy (18.3 kJ/mol). Its drying time is nearly 10% less than that of fluidized bed drying. Even this value is only about 1/4 of blast drying oven. Experimental results show that most of the free water can be removed in a shorter time in the stage of drying speed reduction in cyclone, especially in the initial stage of drying at the same temperature in the low-temperature zone (60 to 80 ℃). It was found that the cyclone drying technology can dry biomass particles in a short time with low energy consumption.

1 Introduction

With the increasing energy and environmental issues caused by the use of fossil fuels, the exploitation of clean and renewable energy sources has attracted great attention worldwide [1]. Biomass such as agricultural residues is considered a potential alternative to fossil fuels due to its advantages in resource renewability and carbon neutrality [2]. Cereal straw is the largest biomass feedstock in the world among the agricultural residues [3] while wheat straw is the second largest lignocellulosic material in the world [4]. Therefore, wheat straw biomass is a valuable feedstock

✉ Huiyan Zhang
  hyzhang@seu.edu.cn

1 Key Laboratory of Energy Thermal Conversion
   and Control, Ministry of Education, School of Energy
   and Environment, Southeast University, Nanjing 210096,
   People's Republic of China

2 State Key Laboratory of Clean and Efficient Coal-Fired
   Power Generation and Pollution Control, China Energy
   Investment Corporation Science and Technology Research
   Institute Co., Ltd, Nanjing 210023, China

for the desired low-carbon alternative. Wheat straw biomass is dried for a more efficient combustion in power plants [5] and in pyrolysis reactors to produce bio-oil [6]. However, it normally has a high moisture content with poor thermal conductivity, which is adverse to its thermal utilization [7], and resulting in a significant quantity of energy consumption during the drying process [8, 9]. Normally, raw biomass has an initial moisture content between 50 and 150% (dry basis). High moisture content reduces the calorific value, limits the particles' heating rate, and inhibits temperature rising within the thermal application [10]. Besides, moisture conducts the pyrolysis reaction to a low activation energy path, and promotes the formation of coke and non-condensable gasses [11]. Therefore, drying of wheat straw before thermal conversion process is a crucial stage. Due to the importance of biomass as a promising energy source, efficient drying of biomass is an open question to academia and industry.

At present, various drying devices are designed and applied in the biomass field. According to different heat transfer mechanisms, they can be roughly divided into convection drying, conduction drying, and radiation drying [12]. Flue gas, steam and superheated steam, extraction steam, and solar heating air are common heat

sources in convection and conduction drying systems. The most common types of convection dryers are rotary drum dryers, fluidized bed dryers, pneumatic dryers, solar dryers, and agitated drum dryers [13, 14]. The performance of fluidized bed dryers is limited by particle size, for the reason that particles larger than 50 mm are difficult to fluidize [15]. Microwave drying has been reported that its effectiveness is at least twice that of traditional drying methods for dielectric materials, including food, biological tissue, and wood [16]. However, due to the high cost of equipment, the inability to produce uniform temperature distribution [17], and dielectric properties changing with temperature, the industrial application of large-scale microwave drying is limited [18]. Lots of studies on fruits and agriculture crops have consistently proved that the far-infrared drying time is short and the quality of the final dried products is reasonable [19], but the drying efficiency is poor when drying thicker materials. Taking the cost, land occupation, drying efficiency, and energy consumption into consideration, cyclone drying may be a better choice.

The cyclone drying technology is developed on the basis of the airflow drying technology. In the rotating flow, the hot gas and the solid particles are fully contacted, and then, the drying process was intensified. However, in recent reports [20–22], the structure of cyclonic dryer is similar to devices used in solid–gas separators. Silva et al. [23] used such devices as dryers in their work. In the study of cyclone drying, Corrêa et al. [24] took the conventional solid–gas separator cyclone as a starting point and showed that changes in geometry may increase the residence time of particles. And Oliveira et al. [25] reported the effect of cyclone geometry and process variables on particle residence time and bagasse moisture reduction in cyclone dryers. However, there is rare report on the study of the drying characteristics of the wheat straw in cyclone dryer.

Experiments show that when the structure of the cyclone and the properties of particles change to a certain extent, the particles are no longer rapidly discharged along the helix, but linger in the conical area of the dryer, which is a recirculating motion in a suspended state. The recirculation motion of the suspended state directly increases the processing cycle of the particles, significantly increasing the residence time of the particles in the cyclone. In addition, the interface with other phases can be continuously updated, enabling deep drying. A similar phenomenon of particle suspension motion was found in the research of Shi et al. [26]. The mechanism of particle movement during cyclone drying may partly explain the increased particle residence time by changing the dryer geometry [25]. In addition, in order to further study the influence on particle movement during drying,

it is necessary to investigate the drying mechanism of cyclone drying. It is precisely because of the movement of feedstocks and the characteristics of heat and mass transfer with the medium in this drying method that it achieves a good drying effect. Therefore, the reasons for the improvement of drying efficiency and the internal mechanism of cyclone drying need to be explored. The applicability of this drying method and the drying effect of different kinds of biomass are still worth exploring. However, there are few studies on this aspect, so we choose representative wheat straw for research.

This research aims to reach the efficient drying of wheat straw and explore the drying mathematical model of cyclone drying by the application of a self-designed pilot-scale cyclone dryer. In this work, the drying characteristics and four different drying models of wheat straw were explored in the cyclone dryer. And the results were compared with two traditional drying methods as blast drying oven and cylindrical fluidized bed.

2 Materials and methods

2.1 Sample preparation

The wheat straw comes from Lianyungang City, Jiangsu Province, China. After reaching the laboratory, the moisture content test (dry basis) is carried out by the moisture tester (Model: DHS-10A, Lichen Inc., Shanghai, China), the drying temperature is set to 105 ℃, and the automatic drying mode is adopted. The drying was stopped when the weight of the material remains unchanged. To determine the particle size distribution (PSD) of samples, a tap sieve shaker was set up in the follow of 0.9-, 1.25-, 2.2-, 3-, and 4-mm sieves. The samples were tapped for 6 min. Then, the mass retained on each sieve was weighed.

Spray the calculated amount of water evenly on the chip particles to adjust their initial moisture content (M_0) to 0.67, 1.00, and 1.50 (dry basis). Wet particles were stored in closed containers and kept indoors in a cool place for at least 3 days to allow the particles to reach a uniform moisture content.

2.2 Drying experiments

2.2.1 Experimental system and procedure

The drying experiment was carried out using a self-designed pilot-scale cyclone dryer, and its results were compared with cylindrical fluidized bed drying and blast drying oven drying. The schematic diagram of cyclone dryer is shown in Fig. 1. The characteristic geometry of the
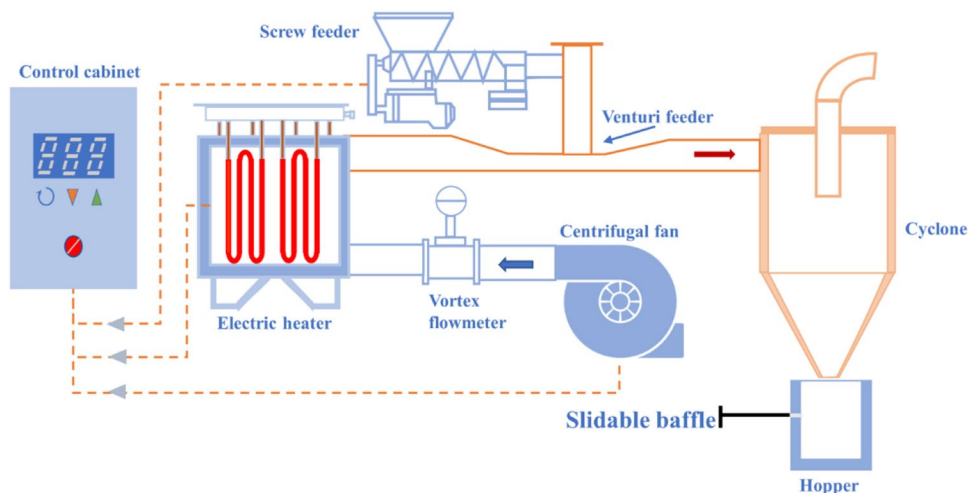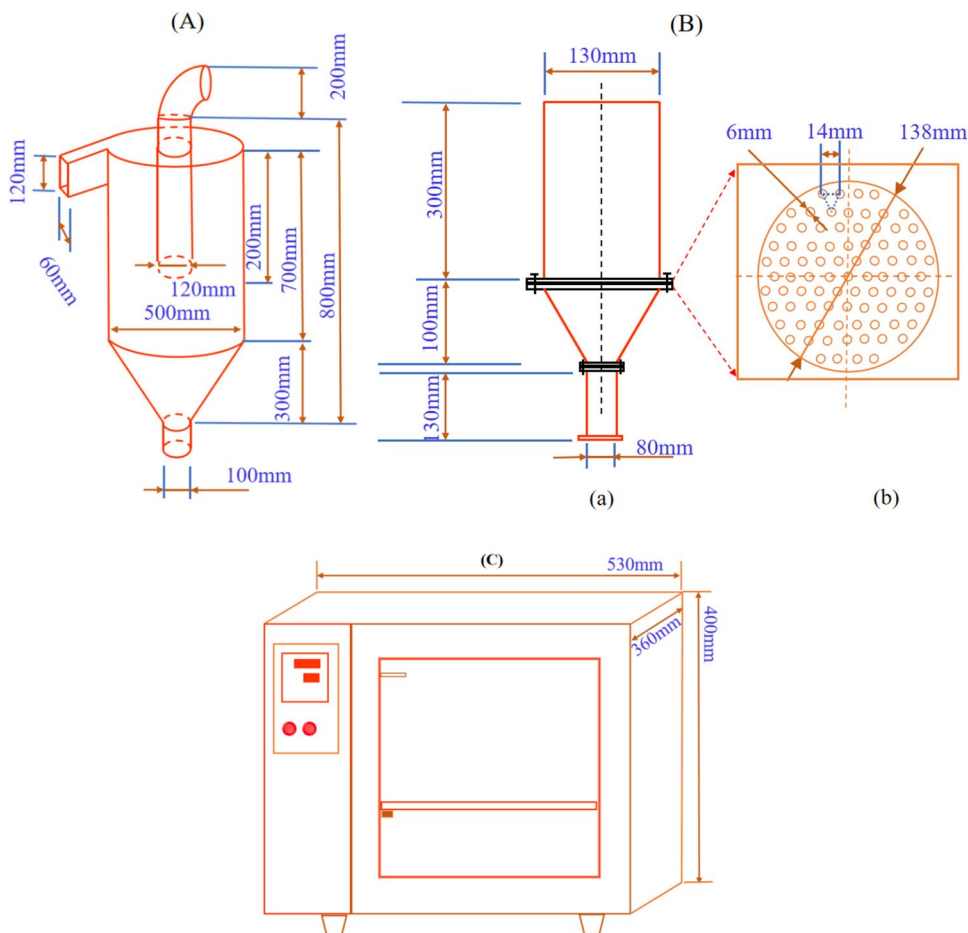
Fig. 1 Schematic picture of cyclone dryer

Fig. 2 Characteristic dimensions of different dryers: **A** cyclone dryer, **B** fluidized bed dryer ((a) schematic diagram of cylindrical fluidized bed dimensions, (b) structure diagrams of gas distributor), **C** blast drying oven

cyclone, the blast drying oven, and the cylindrical fluidized bed is given in Fig. 2.

At the beginning, in the cyclone drying experiment, the effects of the initial moisture content of wheat straw, the temperature of hot air, and the wind speed at the inlet of the dryer on the drying effect were studied. Experimental temperatures of 60, 70, and 80 °C were set by adjusting the power of the electric heater, and the wind speed in the pipeline was controlled by the fan. During the experiment, the fan and electric heater were turned on to reach the required wind speed and the drying chamber was preheated to the required temperature, and then, the feedstock was added.

The drying time of feedstock in the cyclone was recorded. After the drying process, the feedstock was collected and its moisture content was tested in a moisture tester. Repeat the above operation but change the suspension and rotation time of the material in the drying chamber. Finally, according to the obtained data, the drying characteristic curve of the feedstock in the cyclone was plotted.

The cyclone drying system was composed of a blower, an electric heater, an electrical screw feeder, a silo with agitator on the screw feeder, a Venturi feeder, a cyclonic dryer, and a hopper with a slidable baffle in the middle to collect material that falls after the fan is turned off. The air heater is composed of twelve heating tubes, with total power of 12 kW, and the heating power is controlled by a semiconductor module, which can heat the air to 300 ℃. The power of centrifugal fan is 3 kW, which is regulated by frequency converter. The power of the screw feeder is 1.1 kW and the feeding amount can reach 30 kg/h. The duct, the Venturi feeder, and the cyclone were made of stainless steel. Airflow rates were measured by a vortex flowmeter. The entire system was thermally isolated with aluminum silicate insulation cotton (5.0 cm of thickness).

Then, in the cylindrical fluidized bed, the influence of the initial moisture content and temperature of materials on the drying characteristics at a certain wind speed was investigated. The fan and electric heater in the previous cyclone drying experiment were reused in cylindrical fluidized bed drying. The experimental temperature was also set at 60, 70, and 80 °C, and the wheat straw pellets with an initial moisture content of 1.0 (dry basis) were dried. In the fluidized bed, the wind speed was controlled as the sedimentation velocity of the feedstock.

Finally, the drying characteristics of wheat straw particles with an initial moisture content of 1.0 (dry basis) were studied at 60, 70, and 80 °C in a blast drying oven. During the drying process, the air is slowly blown from the bottom to the upper outlet to make the temperature distribution in the box uniform.

During the experiment of different dryers, the drying chamber was preheated to the desired experimental temperature, and then, wheat straw pellets with different moisture contents were dried. After drying, the samples were collected, brought to ambient temperature, sealed in aluminum foil bags, and placed in a desiccator. All tests were repeated in duplicate.

2.3 Drying characteristics

2.3.1 Moisture ratio and drying rate

The moisture ratio (MR) was computed by following the subsequent equation (Eq. (1)) [27]:

$$MR = \frac{M_t - M_e}{M_0 - M_e} \tag{1}$$

M_t, M_0, and M_e are the moisture content (kg water/kg dry matter) at time t (min), the initial moisture content (kg water/kg dry matter), and the equilibrium moisture content (kg water/kg dry matter) of the sample, respectively.

The value of M_e was insignificant, compared to those of M_t and M_0. Therefore, the precedent equation can be simplified into Eq. (2):

$$MR = \frac{M_t}{M_0} \tag{2}$$

The drying rate (DR), which represents the moisture elimination rate during drying, was expressed according to Eq. (3) [28]:

$$DR = \frac{M_{t1} - M_{t2}}{t_2 - t_1} \tag{3}$$

M_{t1} and M_{t2} represent the moisture contents (kg water/kg dry matter) at consecutive times t_1 and t_2 (min). MR data of biomass particles versus time was fitted with four semi-theoretical mathematical drying models listed in Table 1. The model parameters were determined using the trust–region nonlinear regression method. Coefficient of determination (R^2) and root mean square error (RMSE) evaluated the fitting goodness of predicted values to experimental values. Higher R^2 and lower RMSE showed better fitting. The values of RMSE and R^2 were calculated by Eq. (4) and Eq. (5), respectively:

$$RMSE = \sqrt{\frac{1}{N} \sum_{i=1}^{N} (MR_{\text{pre},i} - MR_{\text{exp},i})^2} \tag{4}$$

$$R^2 = 1 - \frac{\sum_{i=1}^{N} (MR_{\text{pre},i} - MR_{\text{exp},i})^2}{\sum_{i=1}^{N} (MR_{\text{exp},i} - \overline{MR_{\text{exp},i}})^2} \tag{5}$$

where $MR_{\text{pre},i}$, $MR_{\text{exp},i}$, and $\overline{MR_{\text{exp},i}}$ are predicted, experimental, and average experimental moisture ratios, respectively; N is the number of observations, and n is the number of drying constants.

Table 1 Semi-theoretical drying kinetics models for isothermal drying condition

Model	Isothermal drying model	Parameters	Reference
Newton	MR = exp(-kt)	k	[11]
Page	MR = exp(-kt^n)	n, k	[29]
Henderson	MR = b*exp(-kt)	b, k	[30]
Logarithmic	MR = a+b*exp(-kt)	a, b, k	[8]

2.3.2 Effective moisture diffusivity

The coefficients of moisture diffusivity (D_{eff}) during drying were calculated based on the second law of Fick. Fick's second law shown in Eq. (6) is a well-known mass-diffusion equation to describe the drying process during the drying rate decreasing stage. It has been widely used to interpret the experimental drying data as the drying process is dominated by internal mass transfer. The mathematical solution of Eq. (6) is shown in Eq. (9) [31].

$$\frac{\partial MR}{\partial t} = \nabla[D_{\text{eff}}(\nabla MR)] \tag{6}$$

The crank's solution for Fick's equation (Eq. (6)) for cylindrical shape material is given in Eq. (7):

$$MR = \frac{M_t - M_e}{M_0 - M_e} = \frac{8}{\pi^2}\sum_{n=1}^{\infty}\frac{4}{b_n^2}\exp(-\frac{D_{\text{eff}}b_n^2 t}{r^2}) \tag{7}$$

where D_{eff} is the effective moisture diffusivity (m²/s), t is the drying time (s), r is the average radius of a sample (m), n is the positive integer, and bn are the roots (2.405, 5.52, 8.654......) of Bessel's function. Effective diffusivity is estimated by considering only the first term of general solution [32], and then, Eq. (7) becomes:

$$MR = \frac{M_t - M_e}{M_0 - M_e} = \sum_{n=1}^{\infty}\frac{4}{b_n^2}\exp(-\frac{D_{\text{eff}}b_n^2 t}{r^2}) \tag{8}$$

Only the first term in Eq. (8) is significant for longer drying times and $n > 1$ and the solution of Fick's equation becomes:

$$MR = \frac{M_t - M_e}{M_0 - M_e} = \frac{4}{b_1^2}\exp(-\frac{b_1^2 D_{\text{eff}} t}{r^2}) \tag{9}$$

where b_1 is 2.405 from the Bessel function. A simplified solution for Eq. (9) can be written in a logarithmic form as follows:

$$\ln MR = A - B \times t \tag{10}$$

where B is the line slope which is related to D_{eff}.

$$B = \frac{b_1^2 D_{\text{eff}}}{r^2} \tag{11}$$

The coefficient of moisture diffusivity (D_{eff}) was computed from the mathematical expression of the slope of the curve ln (MR) versus drying time (Eq. (11)).

2.3.3 Drying activation energy

The temperature dependence of the D_{eff} is generally described by an Arrhenius relationship (Eq. (12)). The drying activation energy can be calculated by plotting $\ln(D_{\text{eff}})$ versus $1 / (T + 273.15)$. The method of calculating E_a is similar to that of calculating D_{eff}.

$$D_{\text{eff}} = D_0\exp(-\frac{E_a}{R(T + 273.15)}) \tag{12}$$

where E_a is the drying activation energy (J/mol), D_0 is the pre-exponential factor (m²/s), T is the drying temperature (°C), and R is the ideal gas constant (J/mol K).

3 Results and discussion

3.1 Size characterization

Figure 3 shows the PSD of ground wheat straw particles. The mass ratio of particles between 1.25 and 2.2 mm is the largest, which is about 27.5 wt.%. While the particle size above 4 mm has the smallest percentage, it is about 12 wt.%. Approximately 82.5–85% of particles were above 1.25 mm sieve. In this study, the particles size above 1.25 mm was used.

3.2 Force analysis of suspended particles in cyclone

In the gas–solid rotary flow field of the cyclone dryer, there is a balance orbit state of the feedstock. When the feedstock reaches this state, it will suspend and rotate in the force balance region. Since the force balance region in the cyclone dryer has a critical particle capacity, when the feed amount exceeds the critical capacity, the particles will change from suspended rotation state to spiral downward separation. The suspended rotation of the particles
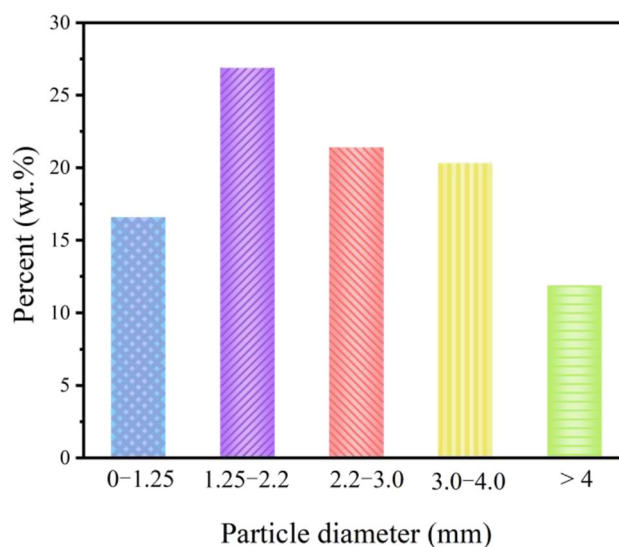

Fig. 3 The PSD of ground wheat straw particles

increases the residence time and the relative velocity of the particle in the suspended region, so that the heat and mass transfer is strengthened.

Figure 4 shows the force analysis of the particles in the cyclone dryer. The particle in rotary motion is mainly supported by friction f, gravity G, wall support force F_N, and air drag force F_D. The resultant force is balanced with the centrifugal force F_C of the particle, so that the particles in the cyclone were in the state of force equilibrium. When Eq. (15) is satisfied, the resultant force on the particle is upward, and the particles are in a suspended state.

$$F_D = \frac{18\mu}{\rho_p d_p^2} \frac{C_D R_e}{24}(u - u_p) \tag{13}$$

$$R_e = \frac{\rho d_p |u_p - u|}{\mu} \tag{14}$$

$$f + F_C \cdot \sin\frac{\alpha}{2} \geq G \cdot \cos\frac{\alpha}{2} + F_D \cdot \cos\frac{\alpha}{2} \tag{15}$$
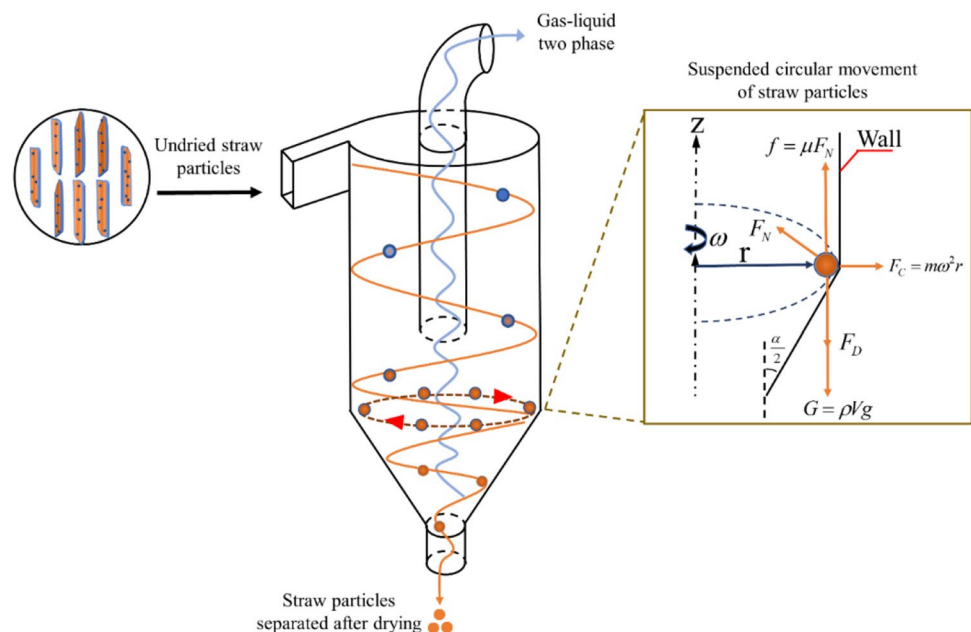
If the particles are continuously added and the critical capacity of the cone section is exceeded, particles will be discharged from the outlet below the dryer. Thus, when the critical capacity of the particles is reached, the feeding will be stopped, and air intake is maintained constantly, so that the particles will suspend and rotate stably in the cone section. At the end of the experiment, when the fan is turned off, the particles will be quickly discharged and collected.

3.3 Analysis of drying characteristic curve

3.3.1 Comparison of drying characteristics of different dryers

Figure 5 presents experimental moisture loss and drying rate for wheat straw particles dried in different dryers. The drying methods were air cyclone drying (ACD), fluidized bed drying (FBD), and blast drying oven (BDO), respectively. From the inspection of Fig. 5a, it was clearly seen that the drying time of the cyclone dryer and the fluidized bed dryer was far less than that of the air blast drying oven dryer, of which the cyclone dryer took the shortest time, and it seemed owning more advantages in the early stage of drying. The drying rate in Fig. 5b showed that the drying rate of feedstock was always in the descending stage during the drying process, which was called as the falling rate period. The drying rate rising stage and constant rate stage were not observed in the experiment. The falling rate period of the drying process of the cyclone dryer and the fluidized bed dryer can be divided into three periods. The first stage is called as the surface free water removal stage. In this stage, water is easy to evaporate during drying, because its saturated vapor pressure is equal to the saturated vapor pressure of pure water at the same temperature and its evaporation mechanism is also consistent with that of pure water surface. The second stage is called as the capillary water removal stage. In this stage, the water inside the capillary tube of the material is removed. The water evaporation is affected by the capillary force, and thus, its saturated vapor pressure is less than the saturated vapor pressure of pure water at the same temperature. The last

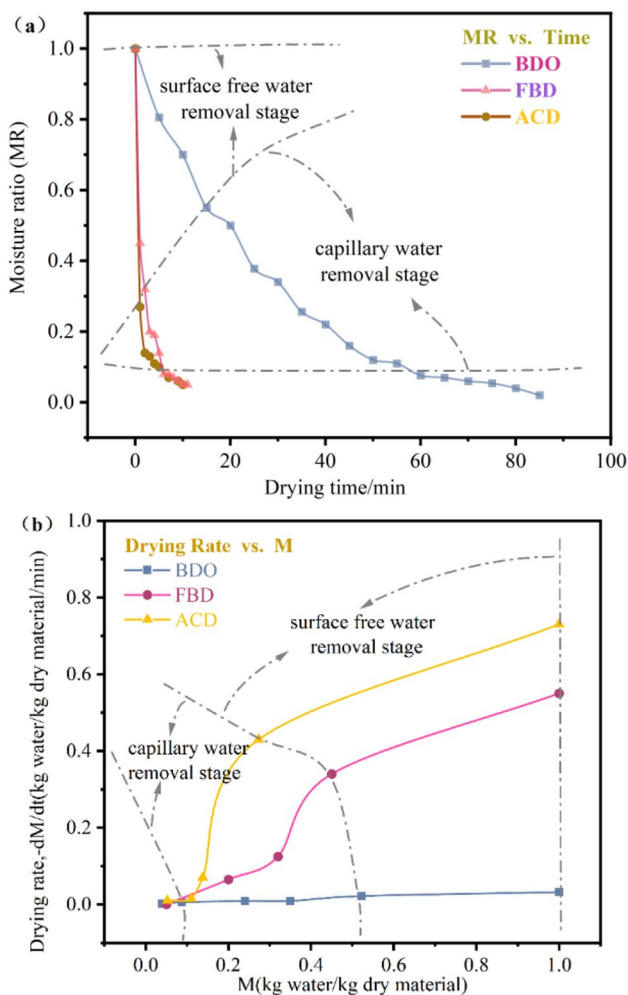Fig. 4 Force analysis of particles in the cyclone dryer

Fig. 5 **a** The mass loss of moisture and **b** drying rate of wheat straw particles in different dryers ($T = 60\ ℃$, $M_0 = 1.0$)

Table 2 Drying conditions in the cyclone

Run	Temperature (°C)	Airflow rate (m/s)	Initial moisture content (kg water/kg dry matter)
E1	60	7	1.0
E2	70	7	1.0
E3	80	7	1.0
E4	60	8	1.0
E5	60	9	1.0
E6	60	7	0.67
E7	60	7	1.50

characteristic curves of the fluidized bed and blast drying oven are respectively shown in Fig. S1 and Fig. S2 in the supporting information.

3.3.2 Cyclone drying

The drying conditions in the cyclone dryer are shown in Table 2. Figure 6a plots the curves of experimental moisture loss and drying rate for ground wheat straw particles with an initial moisture content of 1.0 that were dried at the temperature of 60, 70, and 80 ℃. Moisture content decreased gradually over time, and the greatest decrease occurred in the first 2 min of the drying process. The curves demonstrated typically smooth diffusion-controlled drying behavior under all conditions. It was obvious that the equilibrium moisture content of the material after drying was the lowest at 80 ℃. However, the difference of equilibrium water content at different experimental temperatures was not large, only 0.02 kg water/kg dry solids, so the further experiments were carried out at 60 ℃.

It can be observed that increment in the drying temperature resulted in a clear and uniform increase in the drying rate; then, the drying time was decreased. It is obviously shown in Fig. 6a that the drying was controlled by the falling rate period. The slope of the capillary water removal stage was steeper than that of the surface free water removal stage. The surface free water removal stage was from the beginning of drying to about 0.2–0.3 kg water/kg dry solids and the next stage was the second rapid falling rate cycle. In the drying stages of surface free water and capillary water, the decrease of drying rate lies on the difference of saturated vapor pressure, while in the last stage, the drying rate becomes very low because of the increase of molecular binding water bond energy. Similar scenarios were reported during the dehydration of corn stalks [33] and rice straw [8].

The results obtained in runs of E1, E4, and E5 were used to analyze the effect of airflow rate on moisture ratio and drying rate. Figure 6b depicts the effect of airflow rate on drying characteristics of wheat straw pellets. The maximum velocity of air was 9 m/s, which is 28% higher than the minimum velocity of
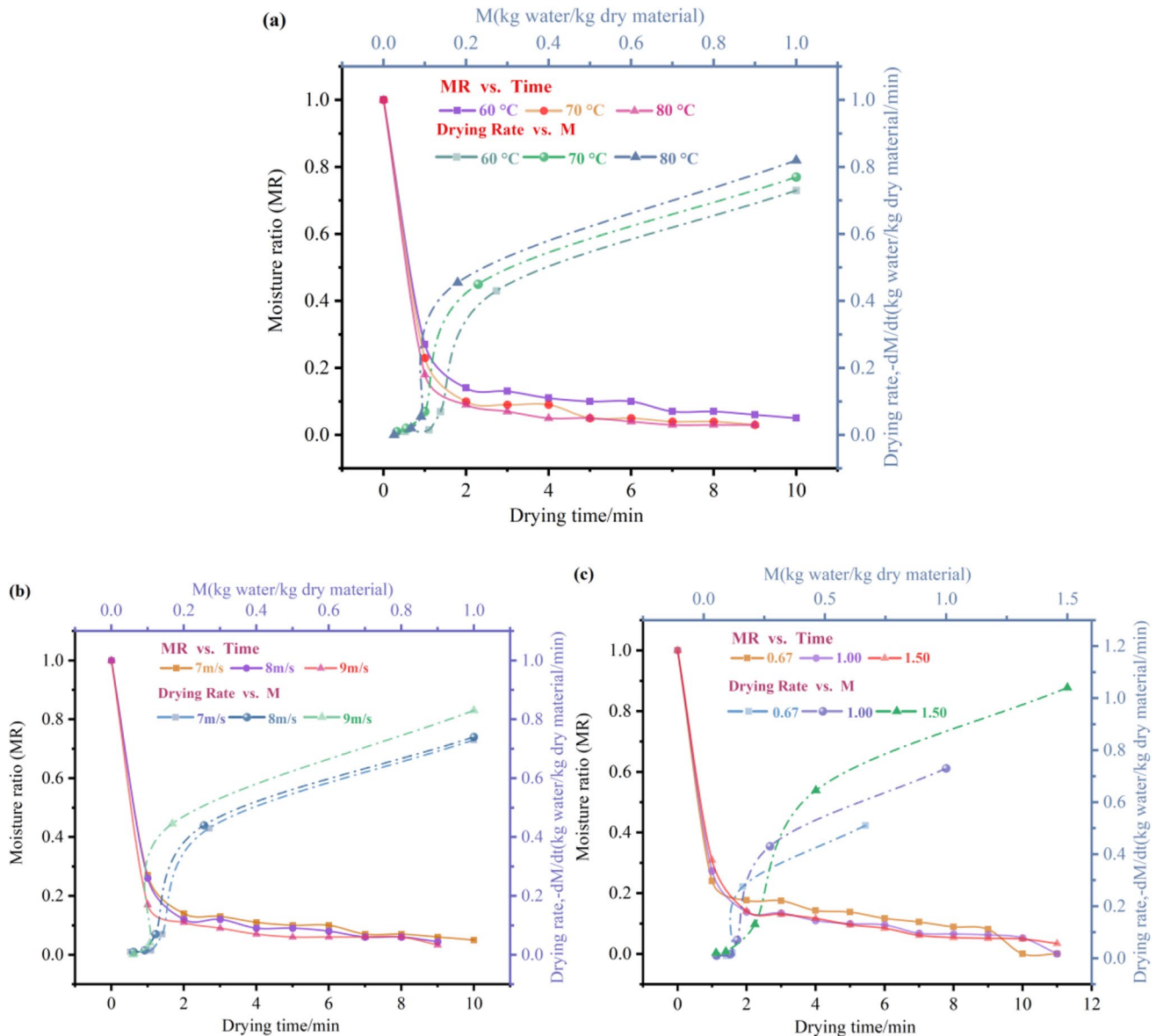
stage is ascribed to the partial removal of molecular bound water, which is quite difficult to evaporate. However, the drying rate of the air blast drying oven only had a quasi-linear relationship with the moisture content.

Before the moisture content reached 0.1 kg water/kg dry material, the drying rate of cyclone drying was obviously higher than that of the other two drying methods. The higher drying rate was attributed to the rapid discharge of large amount of free water which is composed of physical-absorption water on the feedstock surface and capillary. As showed in the drying rate curves, cyclone drying has more advantages in the removal of physical-absorption water than the other two drying methods. The content of bound water in the internal moisture of the feedstock is very low (about 2%), and hardly changes during the drying process. The reason for the difference in the drying characteristics of the cyclone drying and the blast drying oven curve might be the movement state of the particles and the relative speed to the drying airflow. For comparison, the drying

Fig. 6 Moisture loss and drying rate of wheat straw particles in cyclone: **a** at different temperatures ($v = 7$ m/s, $M_0 = 1.0$), **b** at different airflow rates ($M_0 = 1.0$, $T = 60$ ℃), **c** at different moisture contents ($v = 7$ m/s, $T = 60$ ℃)

7 m/s. At the maximum airflow rate, the drying time required for the feedstock to reach the equilibrium moisture content was reduced by about 10%, compared with the minimum airflow rate. The impact of the airflow rate on the drying time at this experimental temperature was not so significant. Besides, with the increase of airflow rate, the moisture content of feedstock declined and the drying rate increased.

The results obtained in runs of E1, E6, and E7 were used to analyze the effect of initial moisture content on moisture ratio and drying rate. The effect of initial moisture content on drying characteristics of wheat straw pellets is shown in Fig. 6c. The feedstock with higher initial moisture content dries faster at the beginning of drying

process. This may be due to that the feedstock with higher initial moisture content contains more free water, so it was easier for the evaporation of water on this part in the early stage of drying. Finally, with the gradual discharge of free water, the gap between the drying rates of different feedstocks gradually decreased and finally disappeared.

3.4 Modeling of drying curves in the cyclone

Four drying models, as listed in Table 1, were used to fit the drying data obtained from the cyclone drying. The best model for describing the drying kinetics of wheat straw particles was chosen as the one with the highest R^2 and the least

RMSE. The statistical analysis results of Page, Newton, Logarithmic, and Henderson models are summarized in Table 3. In the fitting process of experimental data, the "Page model" had the highest R^2 and lowest RMSE.

Figure 7 shows the fitting results at the drying temperatures of 60, 70, and 80 ℃. It can be seen from the figure that the Page model's predicted moisture ratio was very consistent with the drying curve of wheat straw particles. The fitting result reveals that the Page model is an important reference for the industrial application of cyclone dryer.

3.5 Calculation of effective moisture diffusivity and activation energy

The coefficient of moisture diffusivity (D_{eff}) is an essential determinant of mass transfer during drying. The values of D_{eff}) at drying temperatures of 60, 70, and 80 ℃ are given in Fig. 8. Among the three dryers, the D_{eff}) value of ACD was the highest, followed by FBD, and the lowest was BDO. The results also implied that there was a positive correlation between D_{eff})and the processing temperature. The D_{eff}) values of wheat straw increased with the rising temperature, which was consistent with other reports in the literature: 2×10^{-11} to 1×10^{-9} m^2/s for sawdust drying at $65 - 105$ °C [34]; 3.4×10^{-11} to 1.8×10^{-10} for husk of parboiled paddy drying at $50 - 110$ °C [35]; 1.52 to 3.67×10^{-10} m^2/s for rubber wood sawdust drying at $40 - 60$ °C [36].

In fact, during the drying process of BDO, the hot air with low relative humidity constantly passed through the particle gap to conduct heat to the particles. When the moisture inside the particle absorbed heat, the partial pressure of water vapor generated in the particle was increased and drove the moisture move from particle interior to the particle surface. And then the moisture diffused from the surface to the air. Therefore, in the
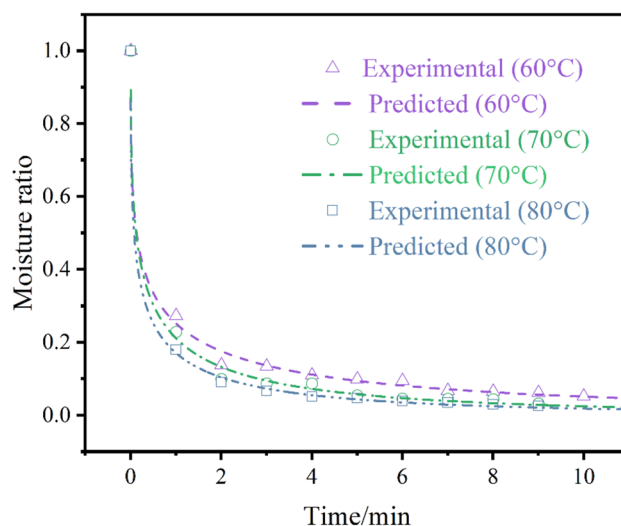

Fig. 7 Comparison of experimental and predicted moisture ratios by the Logarithmic model

flowing air with higher temperature, the heat and mass transfer would be enhanced, leading to higher moisture diffusion. It can be seen from Fig. 8 that cyclone drying displayed the highest D_{eff})value (9.0×10^{-10} m^2/s to 1.3×10^{-9} m^2/s), meaning that the heat and mass transfer effect between particles and airflow was better than the other two dryers. It was possibly ascribed to the higher relative speed between particles and airflow and the high-speed rotation of particles. During the drying process of blast drying oven, the lower D_{eff}) value might be derived from the accumulation of particles, insufficient contact with airflow, and the low relative velocity between particles and airflow. Thus, it can be concluded that higher heating temperature, higher relative velocity, and rapid centrifugal

Table 3 Statistical results obtained from the isothermal models

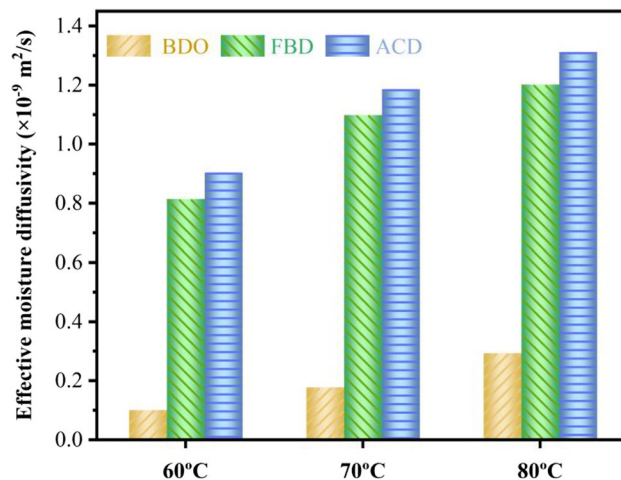| Model	Temperature (°C)	Drying constant (min^{-1})	R^2	RMSE
Page	60	1.379	0.9971	0.01554
	70	1.555	0.9976	0.01525
	80	1.768	0.9995	0.007212
Newton	60	1.061	0.9258	0.07501
	70	1.321	0.9703	0.05109
	80	1.564	0.9814	0.04092
Logarithmic	60	1.517	0.9935	0.02473
	70	1.655	0.9967	0.01927
	80	1.884	0.9978	0.01598
Henderson	60	1.04	0.9262	0.07885
	70	1.314	0.9703	0.05414
	80	1.56	0.9814	0.04339

Fig. 8 Moisture diffusivity of wheat straw subjected to different drying techniques

Fig. 9 **a** Arrhenius type relationship between D_{eff}) and drying temperature. **b** Activation energy of wheat straw particles in ACD, FBD, and BDO
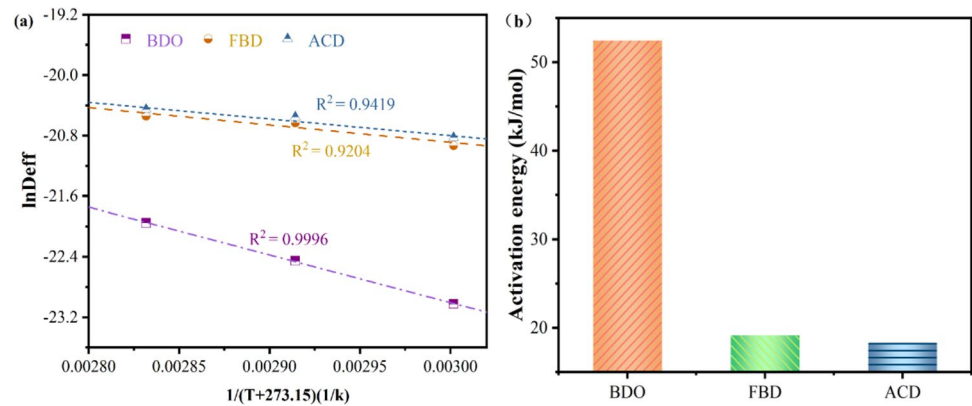
movement of particles will lead to higher drying efficiency and shorter drying time.

The activation energy was determined by Eq. (12). A linear relationship between $\ln(D_{eff}))$ and $1/(T+273.15)$ is presented in Fig. 9 according to the Arrhenius type dependence. Based on the calculation of linear slope, the activation energy values of wheat straw (Fig. 9) were 18.3 kJ/mol in cyclone drying, 19.1 kJ/mol in FBD, and 52.5 kJ/mol in BDO. In this study, the activation energy of wheat straw particles in ACD and FBD was the same order of magnitude as cotton stalk and sawdust proposed in previous studies: 12.3 kJ/mol in poplar sawdust [37]; 14.1 kJ/mol in fir sawdust [38]; 15.1 kJ/mol in cotton stalk [39]. The reason of the lowest activation energy value in ACD can be ascribed to the rapid centrifugal movement of particles and the relatively high speed between particles and airflow, which quickly discharged moisture from the particle surface in the cyclone dryer.

4 Conclusion

This study investigated the drying characteristics of wheat straw particles in a self-designed pilot-scale cyclone dryer, and its results were compared with CFD and BDO. It was found that the drying process under the three conditions mainly occurred during the falling rate, in which moisture transfer was dominated by internal diffusion. Compared with two traditional drying methods, most of the free water was removed in a shorter time in the drying speed reduction stage during cyclone drying. Besides, four drying models were used to fit the drying data in characteristics analysis, and the Page model was found to be the best for describing the cyclone drying. The effective moisture diffusivity ranged from 9.0×10^{-10} to 1.3×10^{-9} m^2/s in cyclone drying, 8.1×10^{-10} to 1.2×10^{-9} m^2/s for cylindrical fluidized bed, and 1.0×10^{-10} to 2.9×10^{-9} m^2/s for blast drying oven within the given temperature range. The values of drying activation energy were 18.3, 19.1, and 52.5.1 kJ/

mol for cyclone, cylindrical fluidized bed, and blast drying oven drying conditions, respectively. Future work will be combined with numerical simulation to study how to optimize the structure of cyclone drying to achieve higher drying efficiency.

Abbreviations ACD: Air cyclone drying; FBD: Fluidized bed drying; BDO: Blast drying oven

Declarations

Ethics approval Not applicable.

Competing interests The authors declare no competing interests.

References

1. Srirangan K, Akawi L, Moo-Young M, Chou P (2012) Towards sustainable production of clean energy carriers from biomass resources. Appl Energy 100:172–186. https://doi.org/10.1016/j.apenergy.2012.05.012
2. Xu Q, Pang S (2008) Mathematical modeling of rotary drying of woody Biomass. Drying Technol 26:1344–1350. https://doi.org/10.1080/07373930802331050
3. Kamarulzaman A, Hasanuzzaman M, Rahim NA (2004) Global potential bioethanol production from wasted crops and crop

residues. Biomass Bioenergy 26:361–375. https://doi.org/10.1016/j.biombioe.2003.08.002

4. Talebnia F, Karakashev D, Angelidaki I (2010) Production of bioethanol from wheat straw: an overview on pretreatment, hydrolysis and fermentation. Bioresour Technol 101:4744–4753. https://doi.org/10.1016/j.biortech.2009.11.080

5. Myllymaa T, Holmberg H, Hillamo H, Laajalehto T, Ahtila P (2014) Wood chip drying in fixed beds: drying kinetics and economics of drying at a municipal combined heat and power plant site. Drying Technol 33:205–215. https://doi.org/10.1080/07373937.2014.945179

6. Uslu A, Faaij PCA, Bergman PCA (2008) Pre-treatment technologies, and their effect on international bioenergy supply chain logistics. Techno-economic evaluation of torrefaction, fast pyrolysis and pelletisation. Energy 33:1206–1223. https://doi.org/10.1016/j.energy.2008.03.007

7. Ramos A, Monteiro E, Rouboa A (2022) Biomass pre-treatment techniques for the production of biofuels using thermal conversion methods – a review. Energy Convers Manage 281 https://doi.org/10.1016/j.enconman.2022.116271.

8. Chen D, Zhang Y, Zhu X (2012) Drying kinetics of rice straw under isothermal and nonisothermal conditions: a comparative study by thermogravimetric analysis. Energy Fuels 26:4189–4194. https://doi.org/10.1021/ef300424n

9. Syahrul S, Hamdullahpur F, Dincer I (2002) Thermal analysis in fluidized bed drying of moist particles. Appl Therm Eng 22:1763–1775. https://doi.org/10.1016/S1359-4311(02)00079-0

10. Rezaei H, Lim CJ, Lau A, Bi X, Sokhansanj S (2017) Development of empirical drying correlations for ground wood chip and ground wood pellet particles. Drying Technol 35:1423–1432. https://doi.org/10.1080/07373937.2016.1198912

11. Chimica D, Napoli U, Tecchio P (2008) Modeling chemical and physical processes of wood and biomass pyrolysis. Prog Energy Combust Sci 34: 47–90. (2008) Modeling chemical and physical processes of wood and biomass pyrolysis. Prog Energy Combust Sci 34:47–90. https://doi.org/10.1016/j.pecs.2006.12.001

12. Yi J, Li X, He J, Duan X (2019) Drying efficiency and product quality of biomass drying: a review. Drying Technol 38:2039–2054. https://doi.org/10.1080/07373937.2019.1628772

13. Fagernäs L, Brammer J, Wilén C, Lauer M, Verhoeff F (2010) Drying of biomass for second generation synfuel production. Biomass Bioenergy 34:1267–1277. https://doi.org/10.1016/j.biombioe.2010.04.005

14. Kamarulzaman A, Hasanuzzaman M, Rahim NA (2021) Global advancement of solar drying technologies and its future prospects: a review. Sol Energy 221:559–582. https://doi.org/10.1016/j.solener.2021.04.056

15. Stenström S (2017) Drying of biofuels from the forest—a review. Drying Technol 35:1167–1181. https://doi.org/10.1080/07373937.2016.1258571

16. Rattanadecho P, Makul N (2015) Microwave-assisted drying: a review of the state-of-the-art. Drying Technol 34:1–38. https://doi.org/10.1080/07373937.2014.957764

17. Zhang J, Luo Y, Liao C, Xiong F, Li X, Sun L, Li X (2016) Theoretical investigation of temperature distribution uniformity in wood during microwave drying in three-port feeding circular resonant cavity. Drying Technol 35:409–416. https://doi.org/10.1080/07373937.2016.1178141

18. Bhattarai S, Oh JH, Choi Y, Oh KC, Euh SH, Kim DH (2012) Microwave drying of sawdust for pellet production: kinetic study under batch mode. J of Biosystems Eng 37:385–397. https://doi.org/10.5307/jbe.2012.37.6.385

19. Riadh MH, Ahmad SAB, Marhaban MH, Soh AC (2014) Infrared heating in food drying: an overview. Drying Technol 33:322–335. https://doi.org/10.1080/07373937.2014.951124

20. Akpinar E, Midilli A, Bicer Y (2003) Single layer drying behaviour of potato slices in a convective cyclone dryer. Energy Convers Manage 44:1689–1705. https://doi.org/10.1016/S0196-8904(02)00171-1

21. Oztop HF, Akpinar EK (2008) Numerical and experimental analysis of moisture transfer for convective drying of some products. Int Commun Heat Mass Transfer 35:169–177. https://doi.org/10.1016/j.icheatmasstransfer.2007.06.005

22. Bunyawanichakul B, MKirkpatrick MP, Sargison JE, Walker GJ (2006) Numerical and experimental studies of the flow field in a cyclone dryer. J Fluids Eng 128:1240–1250. https://doi.org/10.1115/1.2354523

23. Silva MA, Nebra SA (1997) Numerical simulation of drying in a cyclone. Drying Technol 15:1731–1741. https://doi.org/10.1080/07373939708917322

24. Correa JLG, Graminho DR, Silva MA, Nebra SA (2004) Cyclone as a sugar cane bagasse dryer. Chin J Chem Eng 12:826–830

25. de Oliveira LF, Correa JLG, Tosato PG, Borges SV, Alves JGLF, Fonseca BE (2011) Sugarcane bagasse drying in a cyclone: influence of device geometry and operational parameters. Drying Technol 29:946–952. https://doi.org/10.1080/07373937.2011.562062

26. Shi D, Huang Y, Wang H, Yuan W, Fu P (2019) Deoiling of oil-coated catalyst using high-speed suspending self-rotation in cyclone. Sep Purif Technol 210:117–124. https://doi.org/10.1016/j.seppur.2018.03.059

27. Zhou C, Cai Z, Wang X, Feng Y, Xu X, Yagoub AEA, Wahia H, Ma H, Sun Y (2021) Effects of tri-frequency ultrasonic vacuum-assisted ethanol pretreatment on infrared drying efficiency, qualities and microbial safety of scallion stalk slices. Drying Technol 40:2528–2539. https://doi.org/10.1080/07373937.2021.1894572

28. Wang X, Feng Y, Zhou C, Sun Y, Wu B, Yagoub AEA, Aboagarib EAA (2019) Effect of vacuum and ethanol pretreatment on infrared-hot air drying of scallion (Allium fistulosum). Food Chem 295:432–440. https://doi.org/10.1016/j.foodchem.2019.05.145

29. Jensen PD, Temmerman M, Westborg S (2011) Internal particle size distribution of biofuel pellets. Fuel 90:980–986. https://doi.org/10.1016/j.fuel.2010.11.029

30. Baxter L (2005) Biomass-coal co-combustion: opportunity for affordable renewable energy. Fuel 84:1295–1302. https://doi.org/10.1016/j.fuel.2004.09.023

31. Murali S, Delfiya DSA, Kumar KS, Kumar LRG, Nilavan SE, Amulya PR, Krishnan VS, Alfiya PV, Samuel MP (2021) Mathematical modeling of drying kinetics and quality characteristics of shrimps dried under a solar–LPG hybrid dryer. J Aquat Food Prod Technol 30:561–578. https://doi.org/10.1080/10498850.2021.1901814

32. Zogzas NP, Maroulis ZB (1996) Effective moisture diffusivity estimation from drying data. A comparison between various methods of analysis. Drying Technol 14:1543–1573. https://doi.org/10.1080/07373939608917163

33. Zhang X, Lv W, Wang X, Zhao Z, Lin X, Cheng C, Han J (2013) Airflow drying of corn stalks particles in straight horizontal tube. AMR 864–867:499–502. https://doi.org/10.4028/www.scientific.net/AMR.864-867.499

34. Alvarez P, Shene C (1996) Experimental study of the heat and mass transfer during drying in a fluidized bed dryer. Drying Technol 14:701–718. https://doi.org/10.1080/07373939608917121

35. Igathinathane C, Chattopadhyay PK (1999) Moisture diffusion modelling of drying in parboiled paddy components. Part II: Bran

and husk. J Food Eng 41:89–101. https://doi.org/10.1016/S0260-8774(99)00075-8

36. Srinivasakannan C, Balasubramaniam N (2007) Drying of rubber wood sawdust using tray dryer. Part Sci Technol 24:427–439. https://doi.org/10.1080/02726350600934689

37. Chen D, Zheng Y, Zhu X (2012) Determination of effective moisture diffusivity and drying kinetics for poplar sawdust by thermogravimetric analysis under isothermal condition. Bioresour Technol 107:451–455. https://doi.org/10.1016/j.biortech.2011.12.032

38. Chen D, Zhu X (2011) Thermal reaction mechanism of biomass and determination of activation energy I. drying section. J Fuel Chem Technol 39:580–584. https://doi.org/10.3969/j.issn.0253-2409.2011.08.004

39. Chen D, Zhang D, Zhu X (2011) Heat/mass transfer characteristics and nonisothermal drying kinetics at the first stage of biomass pyrolysis. J Therm Anal Calorim 109:847–854. https://doi.org/10.1007/s10973-011-1790-4